CARBON 46 (2008) 1322–1326

available at www.sciencedirect.com

ScienceDirect

journal homepage: www.elsevier.com/locate/carbon

# Enhanced ablation of small anodes in a carbon nanotube arc plasma

*Abraham J. Fetterman*[a,*], *Yevgeny Raitses*[a], *Michael Keidar*[b]

[a]*Princeton Plasma Physics Laboratory, James Forrestal Campus, P.O. Box 451, Princeton, NJ 08543, United States*
[b]*Mechanical and Aerospace Engineering, George Washington University, Washington, DC 20052, United States*

ARTICLE INFO

*Article history:*
Received 19 March 2008
Accepted 16 May 2008
Available online 7 July 2008

ABSTRACT

The ablation rate of a graphite anode is investigated as a function of anode diameter for a carbon nanotube arc plasma. It is found that anomalously high ablation occurs for small anode diameters. This result is explained by the formation of a positive anode sheath. The increased ablation rate due to this positive anode sheath could imply greater production rate for carbon nanotubes.



## 1. Introduction

The discovery of single-walled carbon nanotubes in 1993 [1–4] sparked significant interest in the scientific community because of the diverse properties of this new material. Nanotubes have been considered for hydrogen storage, capacitor construction, flat-panel displays, material strengthening, micromotors, and many other applications [5]. Nanotubes can be produced in many ways [6], but the atmospheric pressure helium arc discharge remains one of the simplest methods for producing large quantities of single-walled carbon nanotubes (CNTs) [7]. This method continues to see innovation in both production volume and quality of nanotube output [8–11]. In such arc discharges, anode phenomena play an important role in nanotube formation. Anode ablation produces carbon atoms that are ionized to form the plasma, which will eventually condense into CNTs.

A number of previous studies focused on anode phenomena due to spot formation in either vacuum arcs and furnaces, or in high current regimes (>1000 A) [12–14]. The anode process has also been studied theoretically in lower pressure regimes with longer arcs [15]. Surprisingly, the anode process of arc discharges for nanotube applications has received little attention. Keidar et al. [16,17] have developed a rigorous description of this ablation process in the appropriate regime, as long as discharge parameters are known. In this model, the near-anode sheath is assumed to be electron repelling (a so-called "negative anode sheath" or "negative anode fall"). In a negative anode sheath, the plasma potential at the boundary of the anode sheath is higher than the anode potential [18,19]. Conversely, in a positive anode sheath, the anode is electron attracting, and the anode potential is the highest. The sign of the sheath is governed by the need to conduct the discharge current through the sheath, closing the circuit between the plasma and the anode.

Negative and positive anode sheath regimes, and their dependence on discharge parameters, electrode geometry, and configuration are known for different types of gas discharges (e.g. glow discharges, low pressure arcs, etc.) [18–20], but not for short length carbon arcs used in nanotube production. In the Keidar et al. model [16,17], the negative anode sheath governs the anode ablation and, consequently, defines the carbon source in CNT production. A consequence of the negative anode sheath is that power deposition to the anode will be dependent primarily on the plasma temperature, density, and surface area. Because of this, one expects ablation to be maximized for an anode diameter equal to the arc diameter, which maximizes power deposition (surface

* *Corresponding author:*
E-mail address: afetter@pppl.gov (A.J. Fetterman).
0008-6223/$ - see front matter 
doi:10.1016/j.carbon.2008.05.018

area), and minimizes cooling along the anode. In the present work, we show experimentally that by decreasing the anode diameter below a certain threshold diameter, the ablation rate can be increased. We explain this behavior by the transition of the anode sheath from negative to positive (electron attractive), leading to enhanced power deposition on the anode. In Sections 2 and 3, we will describe the experimental setup and our results. In Section 4, we use a zero-order model to show the polarity transition in the anode sheath for small anodes.

## 2. Experimental setup

The experimental setup (Fig. 1) consists of a rod shaped graphite anode, and a disk shaped copper cathode. To test the predicted scaling of the ablation rate, we used graphite anodes that varied in diameter from 0.4 cm to 1.25 cm, and in length from 5 cm to 15 cm. The copper cathode has a substantially larger diameter (5 cm) than the anode, so that it is expected to make contact with the entire arc. The experiment was carried out in a helium atmosphere at 600 Torr, in a 10 inch four-way cross. The chamber was pumped down to 10 mTorr before a helium gas was introduced to the chamber.

The graphite anode was mounted on a motorized linear positioner that was computer controlled. A linear potentiometer attached to the positioner was used to monitor the anode position with respect to the cathode. The arc voltage and current, as well as the potentiometer output voltage, were recorded by a PC-based data acquisition and control system. A computerized negative feedback between the arc voltage and the interelectrode gap was used to maintain constant voltage, and thus a constant gap between the anode and the cathode of about 0.2 cm. To initiate the arc discharge, the graphite anode was brought into contact with the copper cathode. Once the arc is struck, the interelectrode gap is increased at a moderate speed (slow enough that the arc is approximately steady state, but fast enough that the ablation is not significant).

The ablation rate was determined by running the arc in a steady state at constant voltage and current. After running for an allotted time (12 s to 8 min) the anode was removed, measured and weighed. This process was repeated at least three times for each anode, and also two to three times for different anode samples of the same diameter. The error bars for the ablation rate were estimated using the standard deviation of multiple measurements, weighted by the amount of time the arc was running for that measurement.

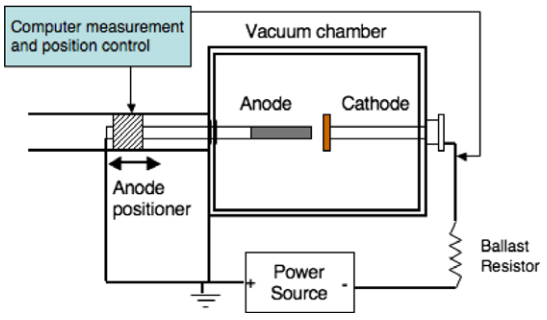


**Fig. 1 – A diagram of the setup used for this experiment.**

## 3. Results and discussion

Experimental ablation rates are shown in Fig. 2. One finds that for anode diameters larger than about 8 mm, the ablation remains small but constant. It is possible that a colder plasma is formed, with larger sheath regions without local thermodynamic equilibrium. This would decrease the ability of the anode to cool the plasma, and allow stable operation of the arc. This suggestion is supported by the measurements of Ostrogorsky et al., who found a decreasing plasma temperature with increasing anode size [21].

The most notable feature of the ablation data is that at low anode diameter (below 6 mm), ablation is as much as three times larger than the predicted values. For example at 70 A, the 4 mm diameter anode lost 35 ± 9 mg/s, while the expected ablation rate was 8 mg/s. We attribute this phenomenon to a change in the behavior of the anode sheath. At large diameters, the anode sheath voltage is negative, as would be predicted. Because the thermal electron flux is greater than the current flux, the electrons are repelled from the anode surface by a negative voltage. When the anode diameter becomes small, though, the opposite effect occurs. The lines of current which are spread uniformly across the arc must converge to reach the anode. This requires a positive anode sheath voltage.

It is possible to estimate this anode sheath voltage by making some assumptions about the plasma. The resistance across the plasma may be written as $\pi r_0^2 \ell \bar{\eta}$, where $\bar{\eta}$ is the average resistivity in the plasma, which is assumed to be a cylinder extending from the anode to the cathode. Then the change in the resistance of the plasma per change in plasma length (d/dl) is

$$\frac{dR}{d\ell} = \pi r_0^2 \bar{\eta}\left(1 + \frac{2\ell}{r_0}\frac{dr_0}{d\ell} + \frac{\ell}{\bar{\eta}}\frac{d\bar{\eta}}{d\ell}\right) \quad (1)$$

If we suppose that the radius and resistivity do not change significantly for small changes in the arc length, then we can calculate the plasma resistance knowing the arc length and change in resistance per change in length. By using data from the linear potentiometer along with the voltage and current data, we can produce a measure of the resistance of the arc as a function of the arc length.

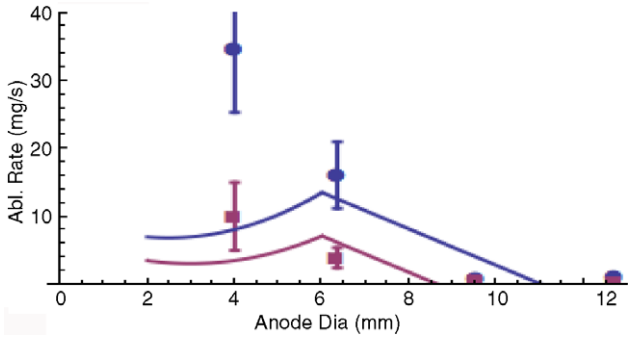


**Fig. 2 – Ablation data and predicted curves. Blue line is theory for 70 A, red line for 50 A. Blue circles are data for 70 A, and red squares are data for 50 A. (For interpretation of the references to color in this figure legend, the reader is referred to the web version of this article.)**

Combining the measurement of the plasma voltage (plasma voltage = total current times arc resistance) with the total measured voltage, we can find the voltage in the combined electrode sheaths. The voltage in the cathodic sheath is essentially constant for a given cathode material, current, and incoming ion species [22], so that this is, up to a constant, indicative of the anode sheath voltage. The arc voltage and anode sheath voltage obtained from this procedure are shown in Fig. 3.

Several features of these graphs are interesting. The electrode voltage (Fig. 3d–f) seems to reach a minimum at an anode diameter near 10 mm. However, for the large diameter anodes the error bars grow to be large. In this case, the arc diameter is probably smaller than the anode diameter, and the location of the arc attachment may be varying across experiments, effecting the measurement of the plasma voltage. The arc diameter and attachment may vary due to an uneven anode surface caused by ablation, or by spot formation processes similar to those recently studied in thermionic cathodes [23]. Moreover, there is unexplained reduction in the ablation rate for the 6.25 mm diameter arc at 50 A. This behavior is repeatable for the single case, but since the effect does not occur over other diameters or currents, the data offers no clear explanation. One trend in Fig. 3d–f that does seem clear is that the electrode voltage increases as the anode diameter is decreased from 10 mm (with the exception of the 6.25 mm diameter anode at 50 A). This is especially the most interesting trend combined with our observation of high ablation for these low diameter anodes.

We will focus on this rise in the electrode potential with decreasing anode diameter. Because the cathode sheath potential is nearly constant, as mentioned earlier, we may assume that this potential rise is increasing in the anode

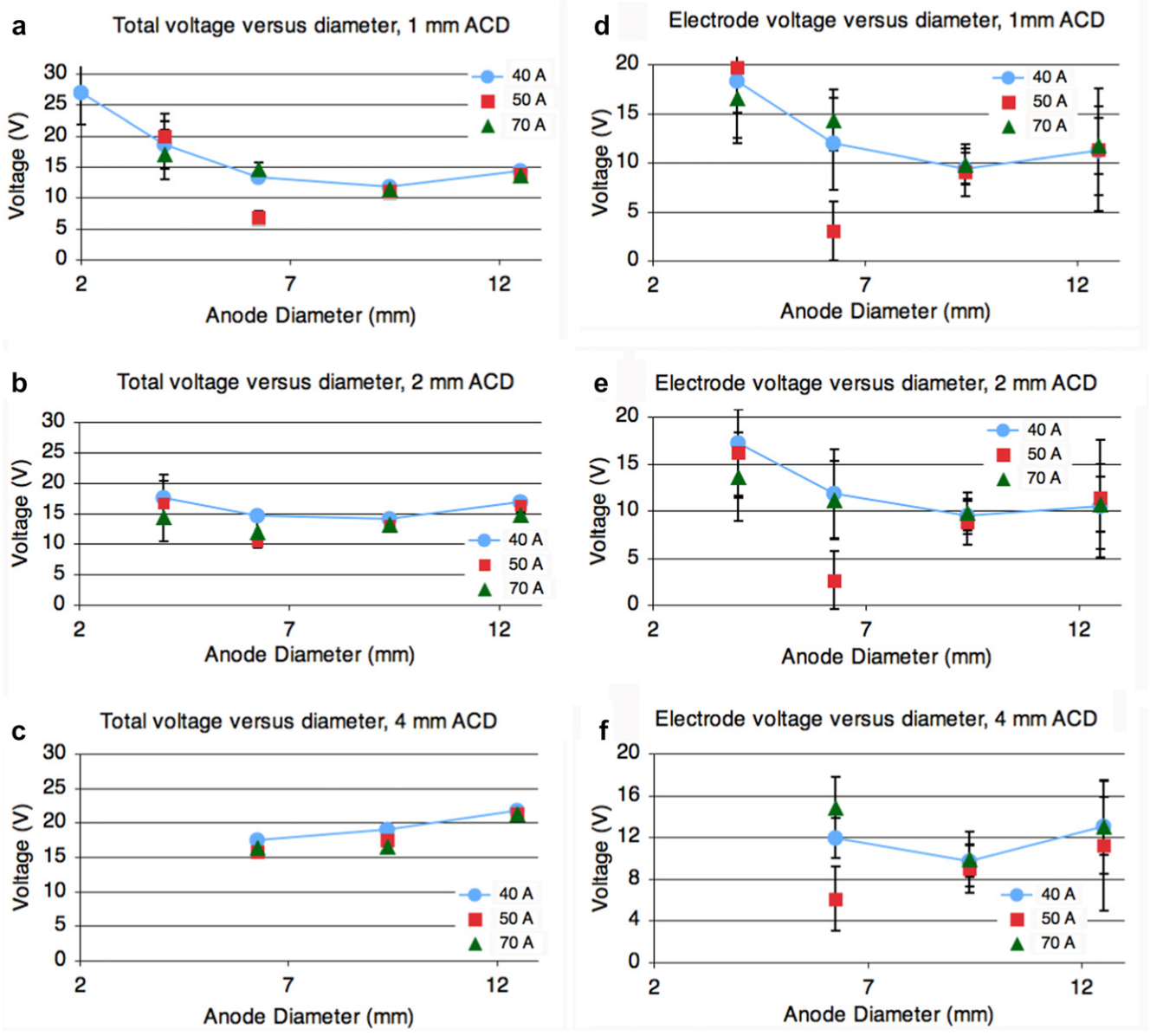


**Fig. 3 – The total measured voltage (a–c) and the voltage in the combined anode and cathode sheaths (d–f), as calculated by removing the estimated plasma voltage. The results are shown for an anode–cathode distance (ACD) of 1 mm, 2 mm, and 4 mm.**

sheath. This increased voltage can increase the current to the anode (required to complete the plasma circuit) in two ways. One way is by increasing the ionization of carbon atoms inside the sheath, leading to a an increased flow of positive ions away from the electrode. The other mechanism is to reshape the plasma in the near-anode region into a cone converging on the anode. This effectively increases the area of the anode so that it can capture a larger amount of electron flux. It is difficult to determine which of these plays a more important role. Theory on the anode sheath voltage due to convergence is especially complicated due to the short length of our arc, as well as its free burning, high-pressure nature [24].

## 4. Anode energy balance

In order to demonstrate how the experimental results differ from the expected scaling, we estimate the ablation rate using a simple anode energy balance. Energy comes to the anode by the electron heat flux from the plasma ($Q_e$) and by thermal conduction from the plasma ($Q_{He}$). It leaves the anode through carbon ablation ($Q_C$) and thermal conduction along the anode ($Q_a$) [17]:

$$Q_e + Q_{He} = Q_C + Q_a. \tag{2}$$

### 4.1. Electron power

The power deposited by the electrons is given by

$$Q_e = (I/e)(2T_e + \phi_e), \tag{3}$$

where $I$ is the total arc current, $e$ is the electron charge, $T_e$ is the plasma electron temperature, and $\phi_e$ is the electron work function.

### 4.2. Heat conduction

The heat conduction from the arc is

$$Q_{He} = \frac{A_a}{L_a}\int_{T_a}^{T_{He}} K dT, \tag{4}$$

where $A_a^{\star}$ is the anode surface area *exposed to the plasma*, $T_{He}$ is the plasma helium temperature, and $T_a$ is the anode temperature. If the arc plasma area is $A_p$, then $A_a^{\star}$ is the minimum of $A_a$ and $A_p$. $L_a$ is the anode sheath scale length, taken to be twice the Helium mean free path [25]. $K$ is the thermal conductivity of Helium (considered the primary heat conductor). An expression for the thermal conductivity may be found by treating Helium as an ideal gas [26]:

$$K(T) = \frac{1}{2}\frac{\sqrt{T/m_{He}}}{\pi r_{He}^2}, \tag{5}$$

where $r_{He}$ is the radius of a helium atom and $m_{He}$ is the Helium atomic mass. We take the scale of the anode sheath to be two Helium mean free paths, $L_a = 2v_{THe}/\nu_{He}$ [25].

### 4.3. Carbon ablation

Carbon ablation leads to the cooling

$$Q_C = (\phi_C + C_p T_a)\frac{\dot{m}_a}{m_C}. \tag{6}$$

$\phi_C$ is the heat of evaporation of carbon, and $C_p$ is the heat capacity of graphite. $\dot{m}_a$ is the rate of change of the anode mass, and $m_C$ is the mass of a carbon atom.

### 4.4. Anode cooling

The anode is a long conductive rod that is cooled by its contact with the helium background gas. If we take the background gas thermal conductivity given in Eq. (5) and constant graphite thermal conductivity $k_C = 85$ W/m K, we find the cooling by the helium per unit length to be

$$\frac{dW}{dx} = \pi r_a^2 k_C \frac{d^2T}{dx^2} = 2\pi\int_0^T K dT, \tag{7}$$

where $r_a$ is the anode radius. Solving this at the surface, for $T = T_a$:

$$Q_a = k_C A_a\left(\frac{8}{15\sqrt{m_{He}}r_{He}^2 k_c A_a}\right)^{1/2} T_a^{5/4}, \tag{8}$$

and here $A_a$ is the total anode area.

### 4.5. Remaining variables

We are now able to solve for the ablation rate, $\dot{m}_a$, using the anode area $A_a$, the cross-sectional area of the arc $A_p$, the anode temperature $T_a$, and arc Helium temperature $T_{He}$. These we have determined from literature for arcs in a Helium atmosphere at 500–600 Torr, with graphite anodes, and current from 40–100 A. These arcs are used for the production of carbon nanotubes, and are expected to have similar plasma attributes as our setup.

Ostrogorsky et al. have measured the anode temperature to be near 3000 K, and the Helium temperature was found to be 6000 K [21]. The discharge used in these experiments had 42 A of arc current. Because the Helium temperature is determined by Joule heating, and so it may vary strongly with current, we use a Helium temperature of 7000 K for our estimation of ablation at 70 A arc current. This was determined by Marcovic et al., in experiments at an arc current of 100 A [27].

We lastly want to estimate the arc radius using the channel model described in Raizer [22]. We may use the Spitzer resistivity $\eta_s \approx 3.3e^2\lambda/T_e^{3/2}m_e^{1/2}$, with electron charge $e$, electron mass $m_e$, and $\lambda \approx 12$. We then can use $\pi r_0^2 = I\eta_s/(V\ell)$, with current $I$ and voltage $V$ determined from our experiments. This yields an arc radius of $r_0 \approx 3$ mm.

### 4.6. Comparison with experiment

A comparison of the theory and experimental data appears in Fig. 2. As the anode diameter is decreased from 6 mm, the theory shows a quadratic fall in the ablation rate due to the decreasing anode surface area exposed to the plasma ($\propto \pi r_a^2$). One sees the expected linear drop-off in the theoretical ablation rate as the anode diameter is increased above 6 mm, due to the increase in the anode surface area available to cooling ($\propto 2\pi r_a$).

It is clear from this graph that there is a disagreement between the theory and experiment. The ablation rate for decreasing anode size rises, rather than the predicted decline.

The formation of a positive anode sheath would increase the power deposited on the anode by electrons, shown in Eq. 3. The anode sheath is on the order of 5–10 V (using Fig. 3d–f), which is on the order of the electron work function (4.6 eV), and temperature (0.6 eV). This implies that the anode sheath voltage would significantly impact the anode ablation rate, as is observed in the experiment.

## 5. Conclusion

Arc discharge experiments were conducted with graphite anodes of different diameters, with a focus on the effect on the carbon mass ablation rate. The expected result of a peak ablation rate where the anode diameter equals the plasma diameter was not found. Instead, the ablation rate increased significantly for small anode sizes. We have shown that this is likely due to the formation of a positive anode sheath.

Because the anode provides the plasma ions, and eventually the raw material for carbon nanotube production, understanding of the anode ablation is critical to understanding the arc operation as a whole. As the Helium electric arc technique for producing SWCNTs continues to be developed, further analysis of the anode region and anode phenomena are necessary to predict and explain arc behavior. This paper shows that there is much left to be known about anode behavior in this particular arc, and that there is an opportunity for increased nanotube production based on greater ablation rates of small anodes.

## Acknowledgements

The authors thank Drs. Stewart Zweben, Phillip Efthimion, and Nathaniel Fisch for their encouraging support of this work. Thanks also to Dick Yager for his technical assistance with the experiment.

## REFERENCES

[1] Monthioux M, Kuznetsov VL. Who should be given credit for the discovery of carbon nanotubes? Carbon 2006;44:1621–3.
[2] Iijima S. Helical microtubules of graphitic carbon. Nature 1991;354:56–8.
[3] Iijima S, Ichihashi T. Single-shell carbon nanotubes of 1 nm diameter. Nature 1993;363:603–5.
[4] Bethune DS, Klang CH, de Vries MS, Gorman G, Savoy R, Vazquez J, et al. Cobalt-catalysed growth of carbon nanotubes with single-atomic-layer walls. Nature 1993;363:605–7.
[5] Baughman RH, Zakhidov AA, de Heer WA. Carbon nanotubes – the route toward applications. Science 2002;297:787–92.
[6] Thostenson E, Ren Z, Chou T. Advances in the science and technology of carbon nanotubes and their composites: a review. Compos Sci Technol 2001;61:1899–912.
[7] Journet C, Maser WK, Bernier P, Loiseau A, de la Chapelle ML, Lefrant S, et al. Large-scale production of single-walled carbon nanotubes by the electric-arc technique. Nature 1997;388:756–8.
[8] Du F, Ma Y, Lv X, Huang Y, Li F, Chen Y. The synthesis of single-walled carbon nanotubes with controlled length and bundle size using the electric arc method. Carbon 2006;44:1327–30.
[9] Doherty SP, Buchholz DB, Chang RPH. Semi-continuous production of multiwalled carbon nanotubes using magnetic field assisted arc furnace. Carbon 2006;44:1511–7.
[10] Mansour A, Razafinimanana M, Monthioux M, Pacheco M, Gleizes A. A significant improvement of both yield and purity during SWCNT synthesis via the electric arc process. Carbon 2007;45:1651–61.
[11] Levchenko I, Ostrikov K, Keidar M, Vladimrov SV. Angular distribution of carbon ion flux in a nanotube array during the plasma process by the Monte Carlo technique. Phys Plasma 2007;14:113504.
[12] Lefort A, Parizet MJ, El-Fassi SE, Abbaoui M. Erosion of graphite electrodes. J Phys D: Appl Phys 1993;26:1239–43.
[13] Beilis II. Anode spot vacuum arc model: graphite anode. IEEE Trans Compon Pack Technol 2000;23:334–40.
[14] Hershcovitch A. Plasma shield for in-air beam processes. Phys Plasma 2008;15:057101.
[15] Alekseyev NI, Dyuzhev GA. Arc discharge with a vaporizable anode: why is the fullerene formation process affected by the kind of buffer gas?. Tech Phys 2001;46:1247–55.
[16] Keidar M, Fan J, Boyd ID, Beilis II. Vaporization of heated materials into discharge plamas. J Appl Phys 2001;89:3095–8.
[17] Keidar M, Waas AM, Raitses Y, Waldorff EI. Modeling of the anodic arc discharge and conditions for single-wall carbon nanotube growth. J Nanosc Nanotechnol 2006;6:1309–14.
[18] Langmuir I, Mott-Smith HM. General Electric Rev 1924;27:449–538. 616, 761, 810.
[19] Kliarfeld BN, Neretina NA. Anode region in a low-pressure gas discharge: 1. Effect of anode shape on sign and magnitude of the anode fall. Soviet Phys Tech Phys 1958;3:271.
[20] Dorf LA, Raitses Y, Fisch NJ. Anode sheath in hall thrusters. Appl Phys Lett 2003;83:2040.
[21] Ostrogorsky AG, Marin C. Heat transfer during production of carbon nanotubes by the electric-arc process. Heat Mass Transf 2006;42:470–7.
[22] Raizer YP. Gas discharge physics. Verlag, New York: Springer; 1991. 245–291.
[23] Benilov M. Stability of direct current transfer to thermionic cathodes: I. Analytical theory. J Phys D: Appl Phys 2007;40:1376–93.
[24] Hoyaux MF. Arc physics. New York: Springer Verlag; 1968. 162–178.
[25] Nemchinsky VA. Anode layer in a high-current arc in atmospheric pressure nitrogen. J Phys D: Appl Phys 2005;38:4082–9.
[26] Kennard EH. Kinetic theory of gases. New York: McGraw-Hill; 1938. 162–165.
[27] Markovic Z, Todorovic-Markovic B, Marinkovic M, Nenadovic T. Temperature measurement of carbon arc plasma in helium. Carbon 2003;41:369–71.